

# Polymeric Micelles Employing Platinum(II) Linker for the Delivery of the Kinase Inhibitor Dactolisib

Haili Shi, Bo Lou, Mies J. van Steenberg, Niels J. Sijbrandi, Wim E. Hennink, and Robbert J. Kok\*

Polymeric micelles are attractive nanocarriers for hydrophobic drug molecules such as the kinase inhibitor dactolisib. Two different poly(ethylene glycol)–poly(acrylic acid) (PEG-*b*-PAA) block-copolymers are synthesized, PEG(5400)-*b*-PAA(2000) and PEG(10000)-*b*-PAA(3700), respectively. Polymeric micelles are formed by self-assembly once dactolisib is conjugated via the ethylenediamine platinum(II) linker (Lx) to the PAA block of the block copolymers. Dactolisib micelles with dactolisib loading content of 17% w/w show good colloidal stability and display sustained release of Lx-dactolisib over 96 h in PBS at 37 °C, while media containing reagents that compete for platinum coordination (e.g., glutathione (GSH) or dithiothreitol (DTT)) effectuate release of the parent inhibitor dactolisib at similar release rates. Dactolisib/lissamine-loaded micelles are internalized by human breast adenocarcinoma cells (MCF-7) in a dose and time-dependent manner as demonstrated by confocal microscopy. Dactolisib-loaded micelles inhibit the PI3K/mTOR signaling pathway at low concentrations ( $400 \times 10^{-9}$  M) and exhibit potent cytotoxicity against MCF-7 cells with  $IC_{50}$  values of  $462 \pm 46$  and  $755 \pm 75 \times 10^{-9}$  M for micelles with either short or longer PEG-*b*-PAA block lengths. In conclusion, dactolisib loaded PEG-*b*-PAA micelles are successfully prepared and hold potential for nanomedicine-based tumor delivery of dactolisib.

highly attractive systems for formulation of hydrophobic drugs. The hydrophobic core can be loaded with high payloads of the drug, and the hydrophilic shell/corona will shield the drug/nanoparticle from opsonization and hence allows the particle to circulate in the body towards its intended target site (i.e., tumor). When small molecule drugs can be entrapped properly into micellar carriers—i.e., adequate drug retention during circulation of the nanoparticles, but drug release upon accumulation at the target site—this type of nanomedicines can have a tremendous impact on the biodistribution and cellular handling of loaded drugs, and hence can largely improve their therapeutic index.<sup>[3]</sup> Drug-loaded nanoparticles can accumulate in tumors via leaky tumors blood vessels, the so-called enhanced-permeability-and-retention (EPR) effect, provided that they circulate sufficiently long.<sup>[4]</sup> The altered intracellular disposition of the drug can overcome multiple-drug resistance (MDR), either due to the intracellular

## 1. Introduction

The application of nanoparticulate drug delivery systems (so-called nanomedicines) for the treatment of cancer provides significant improvements for diagnosis and therapeutic outcome.<sup>[1]</sup> Nanomedicines can overcome several problems associated with the use of low molecular weight drugs and drug candidates, such as poor water solubility, low bioavailability, and nonspecific distribution in the body.<sup>[2]</sup> Particularly polymeric micelles with a hydrophilic shell and a hydrophobic core are


drug reservoir in the nanoparticles or due to avoidance of drug-exporting membrane receptors or metabolizing enzymes.<sup>[3a,5]</sup>

Dactolisib (**Figure 1**) is a dual inhibitor of phosphatidylinositol-3-kinase (PI3K) and mammalian Target of Rapamycin (mTOR) pathways.<sup>[6]</sup> The PI3K/mTOR pathways play a vital role in cell proliferation, growth, survival, and metabolism and contribute to the transformation of cancer cells from a benign, noninvasive state to metastatic tumors which proliferate aggressively.<sup>[7]</sup> Dactolisib is in Phase Ib clinical trials for patients with advanced renal cell carcinoma and Phase II clinical trials for patients with advanced pancreatic neuroendocrine tumors.<sup>[8]</sup> Its clinical applicability is however limited because of poor pharmacokinetics and low tumor accumulation.<sup>[8b]</sup>

The polymeric micelles of the present study consist of block copolymers composed of poly(ethylene glycol) (PEG) and poly(acrylic acid) (PAA). PEG forms the shell and the steric repulsion of PEG chains gives colloidal stability of the micelles. Pegylated nanoparticles generally show prolonged circulation times.<sup>[9]</sup> PAA, as biocompatible and biodegradable polymer,<sup>[10]</sup> has been used as pharmaceutical excipients for oral and ophthalmic drug delivery formulations.<sup>[11]</sup> The pendant carboxylic groups of PAA can be used for drug conjugation, as was shown for cisplatin and other platinum(II) based cytostatic

H. L. Shi, Dr. B. Lou, M. J. van Steenberg, Prof. W. E. Hennink, Dr. R. J. Kok  
Department of Pharmaceutics  
Utrecht Institute for Pharmaceutical Sciences  
Utrecht University  
Universiteitsweg 99, 3584 CG Utrecht, the Netherlands  
E-mail: r.j.kok@uu.nl

Dr. N. J. Sijbrandi  
LinXis B.V  
Cronenburg 75, 1081 GM Amsterdam, the Netherlands

 The ORCID identification number(s) for the author(s) of this article can be found under <https://doi.org/10.1002/ppsc.201900236>.

DOI: 10.1002/ppsc.201900236

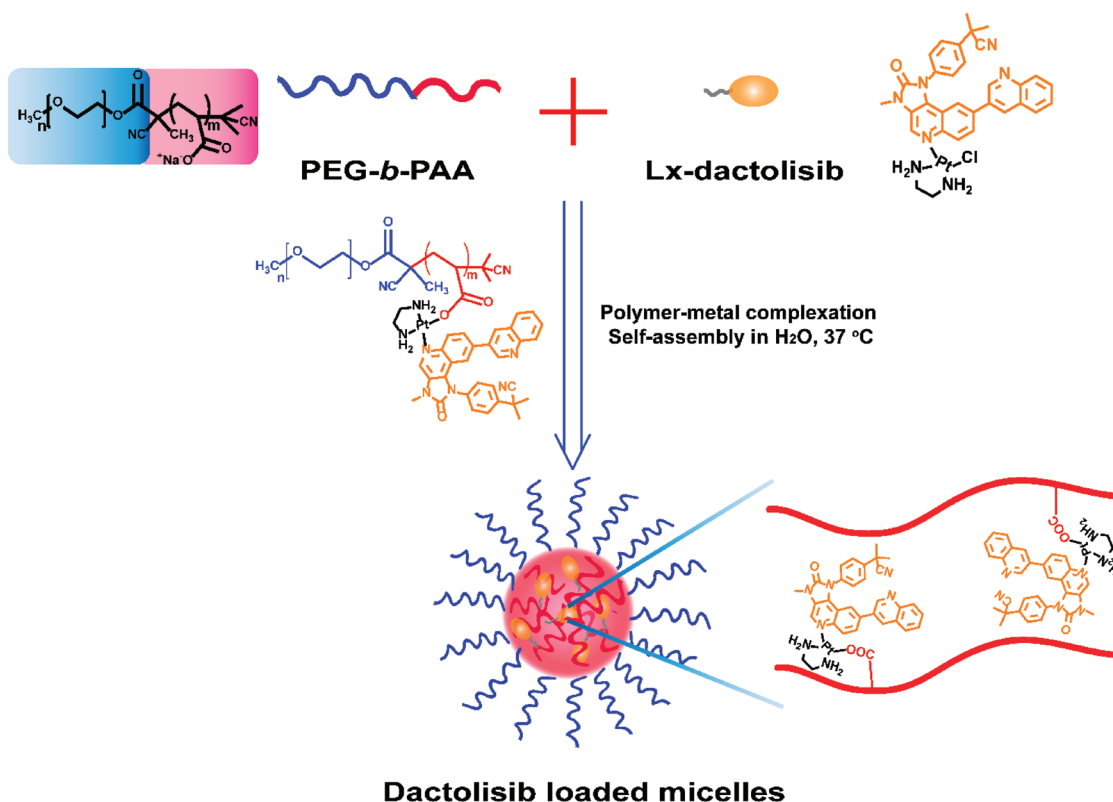


**Figure 1.** Schematic illustration of dactolisib loaded polymeric micelles, prepared through coupling of platinum(II)-linked dactolisib to carboxylate groups of PEG-*b*-PAA block copolymers. Dactolisib: orange color; ethylenediamine-platinum(II) linker (Lx): black color; PEG-*b*-PAA copolymers: PEG block: blue color, PAA block: red color. After coordination of Lx-dactolisib to the PAA block, the hydrophobicity of drug-PAA blocks will facilitate self-assembly of drug-loaded polymers into micelles.

drugs.<sup>[12]</sup> Dactolisib can form coordination bonds with platinum(II) linkers such as ethylenediamine platinum(II), hereafter referred to as Lx,<sup>[13]</sup> which subsequently can be conjugated to PEG-*b*-PAA copolymers. The Lx linker technology is highly versatile as it has been applied for coupling of a range of amphiphilic and hydrophobic drug molecules to different soluble macromolecular carriers, such as antibodies, dendrimers, and protein or peptide carriers.<sup>[14]</sup> Coordination of Lx-dactolisib to carboxylate groups can neutralize the negative charge of the PAA block and results in formation of polymeric micelles with a hydrophobic drug-loaded core surrounded by a hydrophilic PEG shell (Figure 1). Importantly, the drug can be cleaved from the platinum linker by competitive displacement with ligands like glutathione (GSH),<sup>[14e]</sup> which favors the regeneration of the parent dactolisib upon internalization of the micelles.

In the current study, we explored the conjugation of Lx-dactolisib and Lx-lissamine to PEG-*b*-PAA copolymers and their self-assembly into drug or drug/dye loaded polymeric micelles (Figure 1). We explored the stability and drug release from this new type of platinum(II)-linked NDDS and studied their cellular uptake by human breast adenocarcinoma cells (MCF-7) using confocal laser scanning microscopy, while kinase inhibitory effects and in vitro cytotoxicity were examined by phospho-Western blotting and cell viability assays, respectively.

## 2. Results and Discussion

### 2.1. Synthesis and Characterization of PEG-*b*-PAA Block Copolymers

Two PEG-*b*-PAA-CTA block copolymers with different molecular weights were synthesized by reversible addition fragmentation chain transfer (RAFT) polymerization: PEG(5400)-*b*-PAA(2000)-CTA and PEG(10 000)-*b*-PAA(3700)-CTA. PEG(5400)-*b*-PAA(2000)-CTA and PEG(10 000)-*b*-PAA(3700)-CTA were obtained in high yields of 86% and 89%, respectively (Table 1). Based on <sup>1</sup>H-NMR analysis, the acrylic acid conversions were >98% for both polymers. The degrees of polymerization of acrylic acid for PEG(5400)-*b*-PAA(2000)-CTA and PEG(10 000)-*b*-PAA(3700)-CTA calculated using <sup>1</sup>H-NMR spectra, by comparing the integral areas of the protons of the methylene units in PEG (–OCH<sub>2</sub>CH<sub>2</sub>–: δ = 3.73 ppm) and the methine groups of acrylic acid (–CHCOOH: δ = 2.42 ppm) (Figures S4 and S5, Supporting Information, upper panel), were 28 and 52, respectively. The *M<sub>n</sub>* (number-average molar weight) calculated from the <sup>1</sup>H-NMR spectra was 7400 g mol<sup>–1</sup> for PEG(5400)-*b*-PAA(2000)-CTA and 13 700 g mol<sup>–1</sup> for PEG(10 000)-*b*-PAA(3700)-CTA, respectively. The *M<sub>n</sub>* (number-average molar weight) values determined by gel permeation chromatography (GPC) were 6700 g mol<sup>–1</sup> for PEG(5400)-*b*-PAA(2000)-CTA and 12 700 g mol<sup>–1</sup> for

**Table 1.** Characteristics of PEG-*b*-PAA-CTA block copolymers in this study.

Polymer	Feed [AA]:[PEG-CTA]:[ACPA] <sup>a)</sup>	AA monomer conversion [%] <sup>b)</sup>	Yield [%] <sup>c)</sup>	$M_{n,NMR}$ [ $10^3$ g mol <sup>-1</sup> ] <sup>d)</sup>	$M_{n,GPC}$ [ $10^3$ g mol <sup>-1</sup> ] <sup>e)</sup>	$M_w/M_n$ <sup>f)</sup>
PEG(5400)- <i>b</i> -PAA(2000)-CTA	28:1:0.1	98	86	7.4	6.7	1.10
PEG(10 000)- <i>b</i> -PAA(3700)-CTA	52:1:0.1	100	89	13.7	12.7	1.07

<sup>a)</sup>AA: acrylic acid; PEG-CTA: poly(ethylene glycol) methyl ether 4-cyano-4-[(dodecyl sulfanyl thiocarbonyl) sulfanyl] pentanoate; ACPA: 4,4-azobis(4-cyanovaleic acid); [AA]:[PEG-CTA]:[ACPA] is the mol:mol:mol feed ratio with  $0.52 \text{ mol L}^{-1}$  [AA] (the molar concentration of AA); <sup>b)</sup>AA monomer conversion was determined by <sup>1</sup>H NMR analysis; <sup>c)</sup>Yield was determined by weight of collected PEG-*b*-PAA-CTA; <sup>d)</sup> $M_{n,NMR}$  calculated from <sup>1</sup>H NMR; <sup>e)</sup> $M_{n,GPC}$  determined by GPC; <sup>f)</sup> $M_w/M_n$ : polydispersity index (PDI).

PEG(10 000)-*b*-PAA(3700)-CTA, respectively (Table 1). Both polymers had narrow molecular weight distributions of around 1.1, as determined by GPC (Figure S6, Supporting Information). Narrow molecular weight distributions are typical for polymers synthesized via controlled radical polymerization methods.<sup>[15]</sup>

AIBN and LPO were used to remove the thiocarbonylthio end group of PEG-*b*-PAA-CTA to form PEG(5400)-*b*-PAA(2000) (referred to as short-polymer) and PEG(10 000)-*b*-PAA(3700) (referred to as long-polymer) via a radical induced reduction process as described previously by Chen et al.<sup>[16]</sup> The color of the polymers before end group removal was yellow, whereas the polymer was white after end group removal. This visual observation suggests that the end group was indeed removed from the end chain of the polymers. The removal of the CTA group was furthermore demonstrated by UV analysis in which the characteristic peak at 306 nm had disappeared after AIBN/LPO treatment (Figure S7, Supporting Information). In addition, the signal at 0.89 ppm in the <sup>1</sup>H-NMR spectra corresponding to the end methyl group of CTA disappeared after removing thiocarbonylthio group (Figures S4 and S5, Supporting Information). As expected, the composition of the copolymers was not altered after the removal of the CTA group, since the relative signals of the methylene units in PEG ( $-\text{OCH}_2\text{CH}_2-$ :  $\delta = 3.73$  ppm) and the methine groups of PAA ( $-\text{CHCOOH}$ :  $\delta = 2.42$  ppm) had not changed (Figures S4 and S5, Supporting Information).

## 2.2. Characterization of Lx-Dactolisib and Lx-Lissamine

The characteristics of Lx-dactolisib and Lx-lissamine were reported elsewhere<sup>[13]</sup> and are summarized in Figure S8 in the Supporting Information.

## 2.3. Preparation and Characterization of Micelles

Coupling of Lx-dactolisib to acrylate groups of PEG-PAA transformed the hydrophilic PAA domain into a hydrophobic block that causes self-assembly of the drug-loaded polymers into micelles. Nonconjugated drug and unmodified PEG-*b*-PAA copolymers as well as drug-polymer conjugates with only a low degree of dactolisib conjugation were removed by ultra-filtration (Figure S3, Supporting Information). Dual loaded fluorescently labeled micelles that contained both Lx-lissamine and Lx-dactolisib (S-lissa&dacto/m and L-lissa&dacto/m) were prepared in a similar way. **Figure 2A** shows a photograph of the different micellar dispersions in water, demonstrating that colloidal stable micelles had been formed that did neither aggregate nor precipitate. The size of micelles prepared with the short-polymer PEG(5400)-*b*-PAA(2000) (S-dacto/m and S-lissa&dacto/m) as determined by dynamic light scattering (DLS) was around 50 nm whereas that with the long-polymer PEG(10 000)-*b*-PAA(3700) (L-dacto/m and L-lissa&dacto/m) was around 130 nm (Table 2). According to transmission

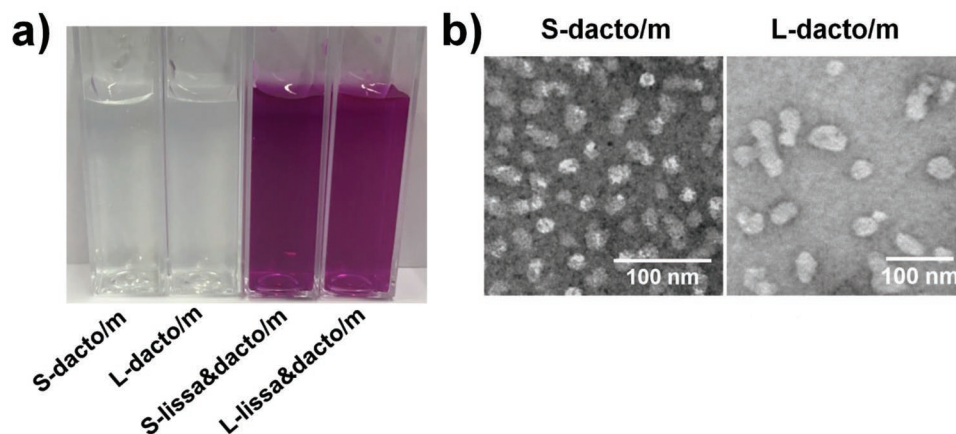


**Figure 2.** Appearance of dactolisib-loaded micelles. a) Photograph of the four types of micellar dispersions in water, S-dacto/m contains  $2.5 \times 10^{-3}$  M dactolisib and  $0.36 \times 10^{-3}$  M PEG(5400)-*b*-PAA(2000)-CTA; L-dacto/m contains  $2.5 \times 10^{-3}$  M dactolisib and  $0.19 \times 10^{-3}$  M PEG(10 000)-*b*-PAA(3700)-CTA; S-lissa&dacto/m contains  $2.0 \times 10^{-3}$  M dactolisib,  $0.5 \times 10^{-3}$  M lissamine and  $0.36 \times 10^{-3}$  M PEG(5400)-*b*-PAA(2000)-CTA; L-lissa&dacto/m contains  $2.0 \times 10^{-3}$  M dactolisib,  $0.5 \times 10^{-3}$  M lissamine and  $0.19 \times 10^{-3}$  M PEG(10 000)-*b*-PAA(3700)-CTA. b) Transmission electron microscopy (TEM) images of S-dacto/m and L-dacto/m after staining with uranyl acetate, scale bar: 100 nm.

**Table 2.** Characteristics of Drug Loaded Polymeric Micelles. Mean Values with Corresponding Standard Deviations are shown ( $n = 3$ ).

Entry	DLS Size [nm] <sup>a)</sup>	PD <sup>b)</sup>	TEM Size [nm] <sup>c)</sup>	Zeta Potential [mV]	LC% <sup>d)</sup>	LE% <sup>e)</sup>
S-dacto/m	57 ± 0	0.19 ± 0.01	22 ± 3	-7.6 ± 0.1	16.5 ± 0.1	50.7 ± 0.5
S-lissa&dacto/m	49 ± 0	0.23 ± 0.01	–	-6.9 ± 0.6	–	–
L-dacto/m	132 ± 1	0.21 ± 0.01	40 ± 9	-5.7 ± 0.2	18.7 ± 0.2	53.4 ± 0.6
L-lissa&dacto/m	130 ± 2	0.22 ± 0.02	–	-7.1 ± 0.2	–	–

<sup>a)</sup>Size determined by DLS; <sup>b)</sup>PDI: polydispersity index, determined by DLS; <sup>c)</sup>Size determined by TEM; <sup>d)</sup>LC: loading capacity, determined using UPLC; <sup>e)</sup>LE: loading efficiency, determined by UPLC.

electron microscope (TEM) analysis, the formed S-dacto/m and L-dacto/m micelles were monodisperse, although their appearance was not spherical (Figure 2B). Notably, the size of the S-dacto/m and L-dacto/m micelles observed using TEM was 22 and 40 nm, respectively (Table 2). The difference in size between the two types of micelles in TEM is most likely due to the longer PAA domain of PEG(10 000)-*b*-PAA(3700) polymer, thus creating a larger core of the micelles after conjugation of Lx-dactolisib. In addition, micelles are dehydrated during sample preparation for TEM analysis, and therefore only the core of micelles is stained with uranyl acetate.<sup>[17]</sup> The core of the micelles most likely consists of a mixed-phase nanogel structure due to the presence of relatively hydrophilic domains (i.e., nonreacted PAA groups) and more hydrophobic domains (i.e., after conjugation of Lx-dactolisib to the copolymers). DLS further provided information on the hydrodynamic radius of the micelles, which is the resultant of both the core of the micelles and the hydrophilic PEG corona. The polydispersity (PDI) of the four micellar dispersions was around 0.2 (Table 2, as determined by DLS), indicating that the different micelles had a narrow size distribution.<sup>[18]</sup> The zeta potential of the micelles at pH 7.4 was slightly negative (around -5 to -8 mV), which is in agreement with abundance of carboxylic acid groups in the PAA domain. Previous publications on cisplatin loaded PEG-*b*-poly(L-glutamic acid) micelles also reported a slightly negative zeta potential of the developed micelles.<sup>[19]</sup> Drug loading content of the micelles was determined by disruption of the drug-platinum(II) coordination bond by adding an excess of a platinophilic ligand, thiocyanate (SCN<sup>-</sup>), after incubation at 80 °C for 24 h.<sup>[20]</sup> The drug loading capacity at a

feed ratio of [Lx-dactolisib]/[COO<sup>-</sup>] = 0.5 (mol/mol) was 16.5% and 18.7% for S-dacto/m and L-dacto/m micelles, respectively (Table 2). This is in close range of the drug loading content of other polymeric micelles such as nanoplatin (NC6004).<sup>[23]</sup> The obtained drug loading contents correspond to a drug loading efficiency of approximately 50% implying that about 25% of the carboxylate groups of the PAA block was modified with Lx-dactolisib groups. Thus, the number of appended Lx-dactolisib groups was 7 dactolisib/polymer for the short polymer, while 13 Lx-dactolisib groups were conjugated to the long polymer.

#### 2.4. Micellar Stability

Colloidal instability and drug leakage are two major problems encountered after in vivo administration of such particle systems. We therefore studied the stability of dactolisib micelles in different release media at 37 °C. Colloidal stability of micelles was studied by DLS. **Figure 3** shows that there was a slight increase in the hydrodynamic diameter and PDI for both S-dacto/m and L-dacto/m after 48 h incubation in PBS. Possibly, this increase can be attributed to partial release of Lx-dactolisib in PBS as discussed below in the section on dactolisib release.

#### 2.5. In Vitro Release of Dactolisib

The in vitro release of dactolisib from micelles was studied in Milli Q water, PBS, PBS containing GSH at a concentration matching intracellular conditions ( $10 \times 10^{-3}$  M) or PBS

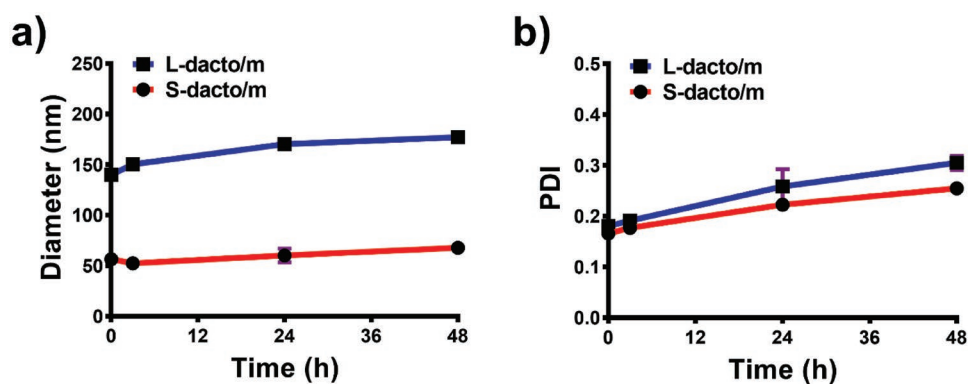


**Figure 3.** Colloidal stability studies dactolisib-loaded micelles incubated in PBS at 37 °C for 48 h. a) Variation in the hydrodynamic diameter of micelles determined by DLS. b) Variation in PDI of micelles determined by DLS.

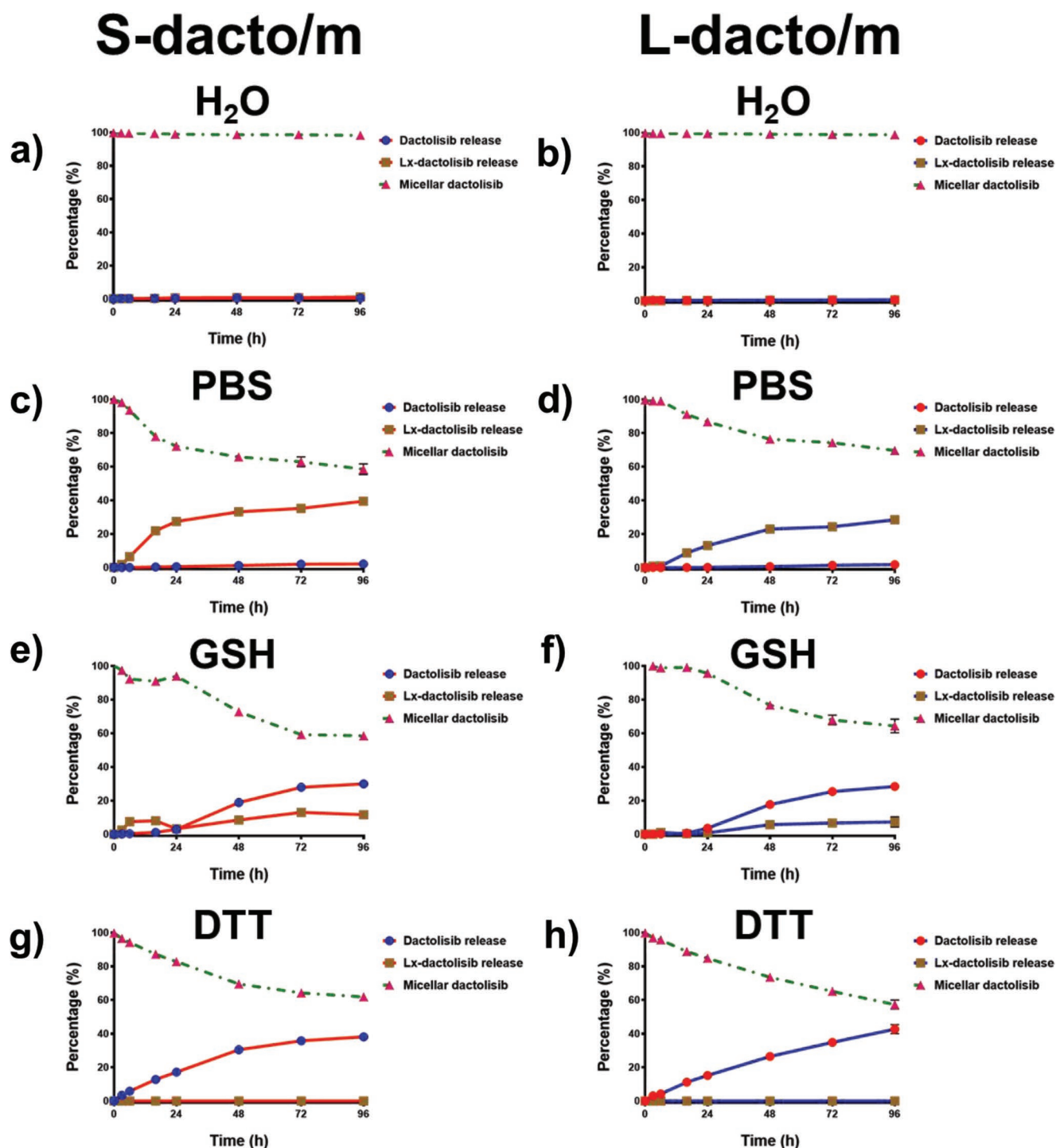


**Figure 4.** In vitro release studies under sink conditions. a,b) Release profile of dactolisib and Lx-dactolisib from S-dacto/m and L-dacto/m micelles in Milli Q water with 1% v/v Tween80 at 37 °C for 96 h. c,d) Release profile of dactolisib and Lx-dactolisib from S-dacto/m and L-dacto/m micelles in PBS with 1% v/v Tween80 at 37 °C for 96 h. e,f) Release profile of dactolisib and Lx-dactolisib from S-dacto/m and L-dacto/m micelles in PBS containing  $10 \times 10^{-3}$  M GSH and with 1% v/v Tween80 at 37 °C for 96 h. g,h) Release profile of dactolisib and Lx-dactolisib from S-dacto/m and L-dacto/m micelles in PBS containing  $10 \times 10^{-3}$  M DTT and with 1% v/v Tween80 at 37 °C for 96 h. The data are shown as the mean  $\pm$  S.D. ( $n = 3$ ).

containing stronger platinophilic agent dithiothreitol (DTT). The amount of free dactolisib and Lx-dactolisib released from S-dacto/m and L-dacto/m in Milli Q water after 96 h incubation was very low, and around 98% drug was remained in both

micelles (Figure 4a,b). Hence, in the absence of competing ligands, dactolisib is efficiently retained in the core of micelles. Upon incubation in PBS at 37 °C, only low amounts of free dactolisib were released amounting to around 2% after 96 h. On the

other hand, Lx-dactolisib was released up to 39% (S-dacto/m) or 28% (L-dacto/m), respectively, at an average release rate of 9%/day for S-dacto/m and 7%/day for L-dacto/m (Figure 4c,d). A plausible explanation for the release of dactolisib-Lx in PBS is chloride-driven competitive displacement, which has been observed for cisplatin and DACHPt from PEG-*b*-poly(Glu) micelles.<sup>[12a,21]</sup> Upon release of Lx-dactolisib, the hydrophilicity of the core increases and the increase of negatively charged acrylate groups will result in an increase of the core of the micelles due to electrostatic repulsion, as shown in Figure 3.<sup>[9c]</sup>

Addition of GSH or DTT to the medium did not increase the total release rate of dactolisib from the micelles or, inversely, the amount of dactolisib remaining in the micelles (Figure 4, dotted lines), but converted the released compound into the parent dactolisib. While DTT was capable of fully releasing dactolisib from the linker,  $10 \times 10^{-3}$  M GSH converted roughly 80% of the cumulatively released Lx-dactolisib to free dactolisib (Figure 4e–h). The observed release of dactolisib from the platinum(II) linker in the presence of thiol-containing compounds is in good agreement with previous studies on soluble Lx-drug conjugates based on protein and polymer backbones.<sup>[13,14d,22]</sup> On the other hand, the observed release of Lx-dactolisib from PAA is in good agreement with the release rates of cisplatin and DACHPt from PEG-*b*-poly(Glu) micelles.<sup>[23]</sup> A likely release mechanism of dactolisib from PEG-*b*-PAA polymeric micelles thus contains two steps. First, chloride ions (which are most abundant) and other platinophilic molecules such as GSH penetrate into the micellar core and disrupt the coordination bond between the PAA block of the polymer and the platinum linker. Next, the Lx-drug complex diffuses out of the core of the micelles, and the bond between platinum linker and dactolisib is cleaved by GSH via competitive displacement.

The slow release of dactolisib-Lx in presence of chloride ions is comparable to the release of cisplatin from PEG-polyglu micelles<sup>[12a,21,23]</sup> which have similar drug linkage chemistry. We therefore expect that dactolisib micelles will display serum stability comparable to those cisplatin micelles which proved adequate for achieving enhanced tumor accumulation of the incorporated drug.<sup>[23]</sup> In other words, it is likely that the majority of dactolisib will remain attached to the core of the micelles during the circulation phase of the micelles upon systemic (intravenous) injection. Organ and tumor distribution of dactolisib will be guided by the physicochemical properties of the nanocarrier, which will favor accumulation into the tumor microenvironment via EPR. The subsequent fate of the micelles will depend on their handling within the tumor environment, and can either involve drug release within the tumor microenvironment, or active uptake of micelles by tumor cells.

## 2.6. Cellular Uptake of Dactolisib Loaded Micelles

The cellular uptake of the fluorescently labelled micelles by MCF-7 tumor cells was studied using a state-of-the-art imaging platform that enables accurate image analysis of fluorescent particles in adherent cells. The image analysis software is capable of discriminating between intracellular fluorescence and extracellular fluorescence and hence can be used for semi-quantification of the internalized micelles. We investigated

the uptake of S-lissa&dacto/m or L-lissa&dacto/m micelles in MCF-7 cells at a concentration of micelles equivalent to  $5 \times 10^{-6}$  M lissamine for different time periods. The red fluorescence signal representing the internalized micelles was hardly found when the cells were incubated with S-lissa&dacto/m and L-lissa&dacto/m for 15 and 30 min (Figure 5a); however, the signal increased from 13 to  $\approx 200$  a.u. after 180 min incubation (Figure 5b). Uptake of both types of micelles by tumor cells resulted in a punctuate perinuclear staining pattern, indicative of endocytosis and lysosomal accumulation.<sup>[24]</sup> Semiquantitative analysis of the intracellular accumulated lissamine showed similar uptake of both formulations, except for the 180 min timepoint at which uptake of S-lissa&dacto/m was slightly higher than that of L-lissa&dacto/m.

The uptake of fluorescently labeled micelles was further studied at different concentrations corresponding to  $2.5\text{--}40 \times 10^{-6}$  M dactolisib (Figure 5c,d). Saturation of uptake was observed at higher concentrations and the relative intensity at the perimeter of the cells was higher at  $40 \times 10^{-6}$  M than at low concentrations (Figure 5c).<sup>[25]</sup> We observed no difference in uptake of S-lissa&dacto/m and L-lissa&dacto/m micelles.

## 2.7. Cellular Toxicity

The cell viability profiles of MCF-7 cells upon incubation with free dactolisib and dactolisib micelles for three days are shown in Figure 6a. Dose response profiles of all formulations were comparable, with only small differences in  $IC_{50}$  between free dactolisib ( $214 \pm 73 \times 10^{-9}$  M) and dactolisib loaded micelles ( $462 \pm 46$  and  $755 \pm 75 \times 10^{-9}$  M for S-dacto/m and L-dacto/m, respectively). Although the platinum-linker is structurally similar to platinum(II)-based anticancer drugs, the platinum linker is not cytotoxic since its coordination sites are occupied by drug and polymer backbone groups which render it poorly reactive with cellular components.<sup>[14e,22a]</sup> Moreover, dactolisib is active in the nanomolar range while cisplatin toxicity is usually observed in the micromolar range (typically  $25\text{--}100 \times 10^{-6}$  M). The observed  $IC_{50}$  values are therefore much lower than can be attributed to the linker. The difference in cytotoxicity of the two types of micelles can be correlated to the fraction of free drug that becomes available in the medium during the experimental conditions, i.e., the percentage dactolisib that is released from the micelles when incubated at 37 °C in PBS. Small micelles with the shorter polymeric backbone showed the highest release of dactolisib-Lx and also had the highest cytotoxicity (41% vs 30% free dactolisib-Lx for small versus larger micelles).

## 2.8. Phospho-Western Blot Evaluation of PI3K/mTOR Activity

The levels of phosphorylated S6 ribosomal protein and phosphorylated Akt were analyzed by Western blot analysis as a direct marker for inhibitory activities of dactolisib. Phospho-S6 ribosomal protein is one of the downstream mediators of the mTOR pathway while phospho-Akt is a downstream mediator of the PI3K pathway.<sup>[7c,26]</sup> Ultimately, inhibition of both pathways results in a wide range of tumor-inhibitory responses, including inhibition of growth and proliferation of tumor

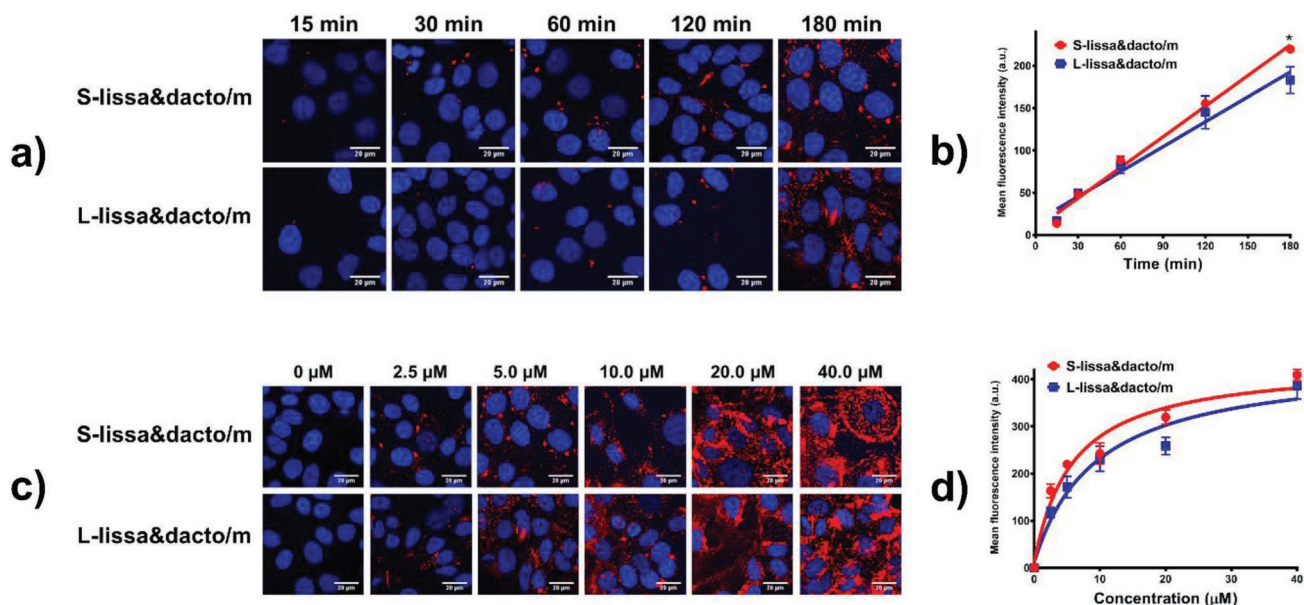


**Figure 5.** Binding and internalization studies with MCF-7 cells. a,b) Time-dependence of internalization of lissamine+dactolisib loaded micelles. a) Confocal microscopic images of MCF-7 cells incubated with S-lissa&dacto/m and L-lissa&dacto/m micelles for 15–180 min; b) semi-quantification of intracellularly accumulated lissamine fluorescence. c,d) Concentration-dependence of lissamine + dactolisib loaded micelles. c) Confocal microscopic images of MCF-7 cells incubated with S-lissa&dacto/m and L-lissa&dacto/m at concentrations of equivalent to  $2.5\text{--}40 \times 10^{-6}$  M lissamine for 3 h at 37 °C. Nuclei were stained in blue with Hoechst 33 342 and lissamine is visible as red spots, bars 20 μm. d) Semi-quantification of intracellularly accumulated lissamine fluorescence. Experiments were performed in triplicate. Quantified data are shown as the mean ± S.D. ( $n = 3$ ), \* indicates  $P < 0.05$ .

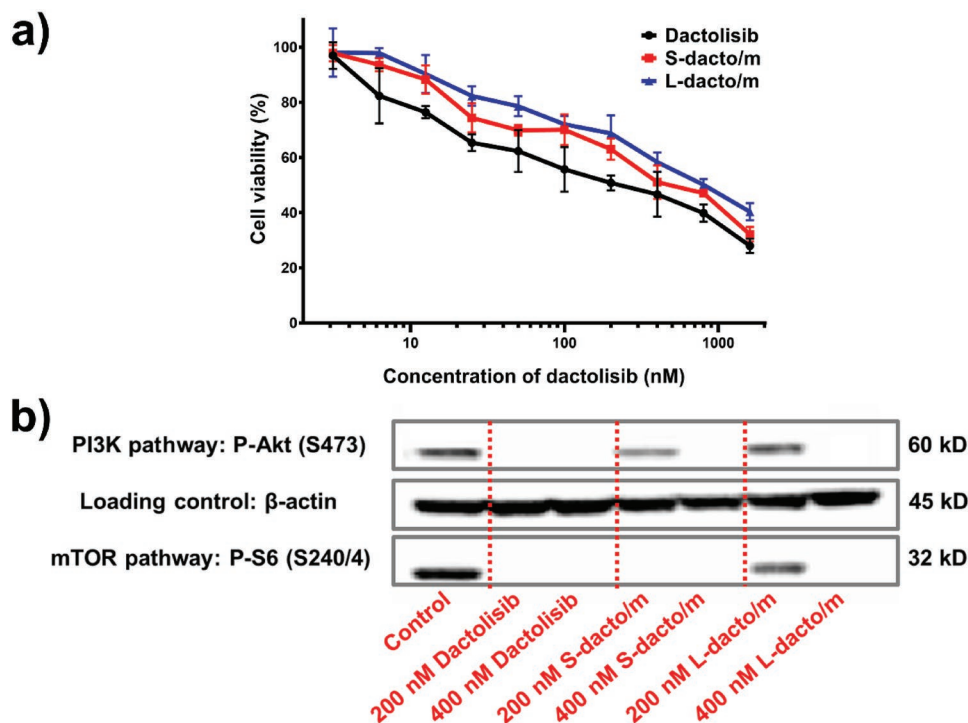


**Figure 6.** a) Viability of MCF-7 cells after incubation with dactolisib formulations. Black curve: free dactolisib; red curve: S-dacto/m; blue curve: L-dacto/m. Cells were incubated with dactolisib formulations for 72 h. Experiments were conducted in triplicate (mean ± S.D.). b) Western blot analysis of PI3K and mTOR activity. Phosphorylation of Ser240/244-S6 (downstream target of mTOR) and Ser473-Akt (downstream target of PI3K) was determined in MCF-7 cells incubated with 200 and  $400 \times 10^{-9}$  M free dactolisib, S-dacto/m or L-dacto/m micelles for 16 h at 37 °C. β-Actin was used as a loading control.

cells. As shown in Figure 6b, free dactolisib and dactolisib micelles decreased the intracellular levels of both phospho-Ser240/244-S6 and of phospho-Ser473-Akt. These results agree with the *in vitro* cytotoxicity results, demonstrating that both kinase inhibitory activity and the final cellular responses can be achieved at nanomolar concentrations of the loaded drug.

First generation polymeric micelles such as poly(ethylene oxide)-*b*-poly(*caprolactone*) micelles had drugs physically loaded in the core. These micellar formulations solubilize hydrophobic drugs and enable the parenteral administration of drugs without the use of organic cosolvents for solubilization of the formulated drug. However, these polymeric micelles have some drawbacks such as poor stability, short blood circulation time, and premature drug leakage.<sup>[27]</sup> Next generation micelles employed different strategies such as physical interactions, conjugation of the drugs to the polymers or chemical core-cross-linking for improving colloidal stability and drug retention in the core of the nanoparticles. For example, PTX loaded methoxy poly(ethylene glycol)-*b*-(*N*-(2-benzoyloxypropyl) methacrylamide) (mPEG-*b*-p(HPMAM-Bz)) polymeric micelles used strong aromatic  $\pi$ - $\pi$  stacking interaction to increase the stability.<sup>[3c,28]</sup> Cisplatin (CDDP) and dichloro(1,2-diaminocyclohexane)platinum(II) (DACHPt) were incorporated in PEG-*b*-poly(*L*-glutamic acid) polymeric micelles via metal-organic coordinative complexation.<sup>[12b,21,29]</sup> CDDP loaded micelles NC-6004 showed significantly improved PK and high tumor accumulation in comparison with free cisplatin after *i.v.* administration.<sup>[12a]</sup> Platinum(II) chemistry was also used to crosslink the polymer chains of micelles, thus increasing the retention of hydrophobic drugs like curcumin in the core.<sup>[30]</sup> In the present article, we used platinum(II) chemistry for conjugation of a hydrophobic drug to a relative hydrophilic core. The resulting Lx-dactolisib modified polymers assemble into micelles which are stabilized by hydrophobic interactions. Dactolisib lacks functional groups that are normally exploited for drug conjugation reactions. Therefore, the use of Lx as linker is an elegant approach because it can coordinate to the aromatic nitrogen of dactolisib and further link the drug to carboxylate groups of the PEG-*b*-PAA block polymer. In addition, the bioreversibility of platinum coordination bonds ensures the regeneration of the parent drug upon interchange with other platinophilic ligands that are present intracellularly at relative high concentrations such as GSH.

### 3. Conclusion

In conclusion, we designed and prepared dactolisib loaded polymeric micelles exploiting platinum linker technology. Dactolisib loaded micelles displayed colloidal stability due to the hydrophobic interactions via the coupled drug molecules in the core of the micelles and released dactolisib in a sustained manner in presence of platinum-competitive ligands. Confocal imaging microscopy studies demonstrated that the micelles can be internalized by tumor cells. Furthermore, dactolisib loaded micelles showed comparable cell toxicity and kinase inhibitory effect to the free drug dactolisib. These findings indicate that dactolisib loaded PEG-*b*-PAA polymeric micelles can be used for a passive tumor targeting strategy.

### 4. Experimental Section

**Materials:** All chemicals were used as bought without any further purification. Dactolisib was purchased from LC Laboratories (Woburn, USA). Poly(ethylene glycol) methyl ether 4-cyano-4-((dodecyl sulfanylthiocarbonyl) sulfanyl) pentanoate (PEG-CTA) ( $M_n$ : 10 000 and 5400 Da), 4,4-azobis(4-cyanovaleric acid) (ACPA), acrylic acid (AA), dichloro(ethylenediamine) platinum(II) [PtCl<sub>2</sub>(en)] (Lx), lissamine rhodamine B sulfonfylchloride, silver nitrate (AgNO<sub>3</sub>), lauroyl peroxide (LPO), 2,2-azobis(2-methylpropionitrile) (AIBN), potassium thiocyanate (KSCN), lithium chloride, L-GSH, DL-DTT, deuterated dimethyl sulfoxide (DMSO-*d*<sub>6</sub>), deuterated methanol (CD<sub>3</sub>OD), tris base, sodium chloride, Tween 80, Tween 20, sodium hydroxide, and formic acid were purchased from Sigma-Aldrich (Zwijndrecht, the Netherlands). Dimethylformamide (DMF), diethyl ether, and acetonitrile were purchased from Biosolve BV (Valkenswaard, the Netherlands). PEGs for GPC calibration were purchased from Polymer Standards Service-USA Inc. Phosphate buffered saline (PBS) pH 7.4 was ordered from B. Braun Melsungen AG, Germany. Hoechst 33 342 solution ( $20 \times 10^{-3}$  M), radio-immunoprecipitation assay (RIPA) buffer, protease and phosphatase inhibitors were ordered from ThermoFisher (Bleiswijk, the Netherlands). 3-(4,5-dimethylthiazol-2-yl)-5-(3-carboxymethoxyphenyl)-2-(4-sulfophenyl)-2H-tetrazolium, inner salt (MTS) cell proliferation assay kit was purchased from Abcam (Cambridge, UK). Phospho-Akt (Ser473) rabbit mAb, phospho-S6 ribosomal protein (Ser240/244) rabbit antibody and  $\beta$ -Actin rabbit mAb were purchased from Cell Signaling Technology (Leiden, the Netherlands). All other cell culture related materials were obtained from Gibco (Grand Island, NY, USA).

**Nuclear Magnetic Resonance (NMR):** <sup>1</sup>H-NMR spectra were recorded using an Agilent 400 MHz spectrometer (Santa Clara, CA, USA) in DMSO-*d*<sub>6</sub> or CD<sub>3</sub>OD at 25 °C. The central line of DMSO-*d*<sub>6</sub> at 2.5 ppm or CD<sub>3</sub>OD at 3.31 ppm was used as the reference line.

**GPC:** The number average molecular weight ( $M_n$ ), weight average molecular weight ( $M_w$ ), and PDI (equal to  $M_w/M_n$ ) of the synthesized polymers were measured using a Waters 2695 Alliance (Waters Associates Inc., Milford, MA, USA) equipped with refractive index (RI) detector and two serial PL aquagel-OH 30, 8  $\mu$ m column (Agilent). PEGs with narrow molecular weights (Polymer Standards Service-USA) were used as standards. 0.1 mol L<sup>-1</sup> Na<sub>2</sub>HPO<sub>4</sub> at pH  $\approx$  9 was used as the eluent with a flow rate of 1.0 mL min<sup>-1</sup> and the column temperature was at 25 °C. The runtime was 30 min.

**Ultraperformance Liquid Chromatography (UPLC):** The purity of the synthesized compounds was determined by UPLC using a Waters ACQUITY system (Waters Associates Inc., Milford, MA, USA) equipped with an ACQUITY UPLC CSH C18 column 1.7  $\mu$ m (2.1  $\times$  50 mm). Water/ acetonitrile (95/5, v/v) with 0.1% formic acid was used as eluent A and acetonitrile with 0.1% formic acid was used as eluent B. A gradient was run from 100% to 40% eluent A in 2.5 min at a flow rate of 0.5 mL min<sup>-1</sup>. The injection volume was 5  $\mu$ L (concentrations ranging from 50 to 200  $\mu$ g mL<sup>-1</sup>) and the runtime was 3.5 min. The column temperature was at 50 °C. The detection wavelength for dactolisib and Lx-dactolisib was 340 nm. The detection wavelength for lissamine, imidazole-lissamine, and Lx-lissamine was 560 nm. Empower Software was used to analyze the chromatograms.

**Liquid Chromatography-Mass Spectrometry (LC-MS):** Lx-dactolisib and Lx-lissamine were determined using a Thermo Finnigan LC system (Thermo Finnigan, San Jose, CA, USA) coupled to a Bruker Q-TOF mass spectrometer (Bremen, Germany) equipped with an electrospray ionization (ESI) source. The column, eluting gradient, flow rate, and injection volume were the same as those for UPLC analyses. Water/ acetonitrile (LC-MS Grade) (95/5, v/v) with 0.1% formic acid was used as eluent A and acetonitrile (LC-MS Grade) with 0.1% formic acid was used as eluent B. The settings of mass analysis were in the positive ionization mode, 70.0 bar nebulizer pressure, 12 l per min drying gas flow rate, 35 °C drying gas temperature, 4.5 kV ESI voltage, and 50 to 3000 *m/z* scan range. The data were analyzed on Bruker Daltonics Data Analysis software. *m/z* Values of analyzed compounds: dactolisib, 470.3, [M+H]<sup>+</sup>, C<sub>30</sub>H<sub>23</sub>N<sub>5</sub>O; Lx-dactolisib, 759.6, [M]<sup>+</sup>, C<sub>32</sub>H<sub>31</sub>ClN<sub>7</sub>OPt; imidazole-lissamine (IMI-lissamine), 666.3, [M+H]<sup>+</sup>, C<sub>33</sub>H<sub>39</sub>N<sub>5</sub>O<sub>6</sub>S<sub>2</sub>; Lx-lissamine, 955.2, [M]<sup>+</sup>, C<sub>35</sub>H<sub>47</sub>ClN<sub>7</sub>O<sub>6</sub>PtS<sub>2</sub>.



**Preparative-High Performance Liquid Chromatography (Prep-HPLC):** A Waters preparative HPLC system using an XBridge BEH C18 OBD Prep column (19 × 150 mm) was used to purify the synthesized Lx-dactolisib and Lx-lissamine. The eluent A and B were the same as those for UPLC analyses. The gradient was 80%–40% eluent A in 30 min with a flow rate of 20 mL min<sup>-1</sup> and the injection volume was 4 mL with a concentration of 20 mg mL<sup>-1</sup>.

**Synthesis and Characterization of Block Copolymers:** RAFT polymerization was adopted to prepare controllable PEG-*b*-PAA block polymers with low PDI. In brief, PEG-*b*-PAA-CTA was synthesized in water using PEG-CTA ( $M_n$ : 10 000 and 5400 Da) as a chain transfer agent, ACPA as a radical initiator and acrylic acid as monomer (Figure S1a, Supporting Information).<sup>[31]</sup> For PEG(5400)-*b*-PAA(2000)-CTA, the polymerization procedure was the following: in a one-neck round-bottom flask, 400 mg of PEG(5400)-CTA ( $1.86 \times 10^{-2}$  mol L<sup>-1</sup>), 2.0 mg of ACPA ( $1.86 \times 10^{-3}$  mol L<sup>-1</sup>), and 150 mg of acrylic acid ( $0.52$  mol L<sup>-1</sup>) were dissolved in 4 mL water. For PEG(10 000)-*b*-PAA(3700)-CTA (referred to as long-polymer), the polymerization procedure was the following: 400 mg of PEG(10 000)-CTA ( $1.00 \times 10^{-2}$  mol L<sup>-1</sup>), 1.0 mg of ACPA ( $1.00 \times 10^{-3}$  mol L<sup>-1</sup>), and 150 mg of acrylic acid ( $0.52$  mol L<sup>-1</sup>) were dissolved in 4 mL water. The mole feed ratio of acrylic acid:PEG(5400)-CTA:ACPA was 28:1:0.1 and the mole feed ratio of acrylic acid:PEG(10 000)-CTA:ACPA was 52:1:0.1. Subsequently, the two mixtures were degassed via three freeze-pump-thaw cycles and immersed in an oil bath thermostated at 70 °C to react for 6 h under a nitrogen atmosphere. Small aliquots ( $\approx 100$   $\mu$ L) were taken at 0 and 6 h to determine the percentage of acrylic acid conversion using <sup>1</sup>H-NMR analysis. The polymerization mixtures were quenched by rapidly freezing in liquid nitrogen. The frozen mixtures were thawed at room temperature and 2 mL methanol was added to the solution. Next, the polymer was precipitated in cold diethyl ether, redissolved in methanol and precipitated in cold diethyl ether. The dissolution/precipitation procedure was repeated three times. Subsequently, the polymers were dried under vacuum at room temperature for 24 h and collected as yellow powders. The  $M_n$  and the degree of polymerization of acrylic acid were calculated using <sup>1</sup>H-NMR spectroscopy (CD<sub>3</sub>OD as solvent) by the relative integration of the protons of PEG-CTA and the vinylic protons of polymerized acrylic acid (Figures S4 and S5, Supporting Information) to yield the  $M_{n,NMR}$ . The  $M_{n,GPC}$  and molar-mass dispersity ( $PDI = M_w/M_n$ ) were determined using GPC as described previously (Figure S6, Supporting Information).

A radical induced reduction procedure was applied for the removal of the thiocarbonylthio end group.<sup>[16,32]</sup> In detail, 100 mg PEG(5400)-*b*-PAA(2000)-CTA was dissolved in 1.5 mL DMF and subsequently AIBN (44.5 mg, 20 molar equivalents) and lauroyl peroxide (LPO) (10.8 mg, 2 molar equivalents) were added to cleave the thiocarbonylthio moiety from the polymeric chains (Figure S1b, Supporting Information). The solution was degassed via three freeze–evacuate–thaw cycles, sealed, and heated at 80 °C to react for 4 h. The solution was cooled and the formed PEG(5400)-*b*-PAA(2000) was precipitated by dropwise addition of the solution into cold diethyl ether. The precipitated polymer was collected by centrifugation and washed three times with diethyl ether. The end group of PEG(10 000)-*b*-PAA(3700)-CTA was removed using the same approach with 20 molar equivalents AIBN and 2 molar equivalents LPO. PEG(5400)-*b*-PAA(2000) (referred to as short-polymer) and PEG(10 000)-*b*-PAA(3700) (referred to as long-polymer) were dried under vacuum at room temperature for 24 h and collected as white powders. UV spectroscopy (UV-2450, Shimadzu, Japan) was used to determine whether the thiocarbonylthio end groups were indeed removed (Figure S7, Supporting Information).

**Synthesis of Lx-Dactolisib:** Lx-dactolisib was synthesized as described in our previous paper.<sup>[13]</sup> Briefly, cis-[Pt(ethylenediamine) nitrate chloride] was synthesized by reacting dichloro(ethylenediamine)platinum(II) [PtCl<sub>2</sub>(en)] (Lx) (750 mg, 2.307 mmol) with AgNO<sub>3</sub> (390 mg, 1 eq) in 15 mL DMF overnight in the dark at room temperature (Figure S2a, Supporting Information). The formed silver chloride precipitate was removed by filtration over a PTFE filter (0.2  $\mu$ m cutoff, 47 mm diameter, Whatman). Dactolisib (400 mg, 0.848 mmol) in 10 mL DMF was heated to

75 °C for complete dissolution. Activated Lx (311.7 mg, 1 eq) in DMF was added to the dactolisib solution and reacted at 60 °C for 24 h (Figure S2b, Supporting Information). UPLC and LC-MS were used to identify the components in the reaction mixture. Subsequently, the reaction solution was diluted 1:3 with reverse osmosis water and injected into a Waters preparative HPLC system to isolate the 1:1 Lx-dactolisib conjugate using the conditions described above. The fractions that contained the aimed product (UPLC and LC-MS analysis) were pooled and freeze-dried.

**Synthesis of Lx-Lissamine:** Lx-lissamine was synthesized in two steps as described previously.<sup>[13]</sup> In brief, imidazole was firstly reacted with lissamine to obtain imidazole-lissamine (IMI-lissamine). Next, Lx was reacted with AgNO<sub>3</sub> to obtain activated Lx that was subsequently reacted with imidazole-lissamine to obtain Lx-lissamine (Figure S2c, Supporting Information).

**Coordination of Lx-Dactolisib and Spontaneous Assembly into Micelles:** Hydrophilic PEG-*b*-PAA block copolymers were reacted with Lx-dactolisib and thus converted into block copolymers with hydrophobic dactolisib-PAA domains that spontaneously assembled into micelles. The protocol for reaction of the polymer with Lx-dactolisib was based on procedure as described for the preparation of cisplatin loaded PEG-*b*-poly(L-glutamic acid) polymeric micelles.<sup>[33]</sup> In brief, Lx-dactolisib (38 mg) was dissolved in 20 mL distilled water by heating at 70 °C for 20 min. Next, the Lx-dactolisib aqueous solution ( $2.5 \times 10^{-3}$  M) was cooled to 37 °C and added dropwise to a solution of either PEG(5400)-*b*-PAA(2000) (short-polymer) or PEG(10 000)-*b*-PAA(3700) (long-polymer) in distilled water ([AA] =  $5.0 \times 10^{-3}$  M; [Lx-dactolisib]:[AA] = 1:2 mol/mol) of which the pH had been adjusted to 7.4 using 0.5 N NaOH (Figure S3, Supporting Information). The reaction solution was incubated for 16 h at 37 °C until micelles were formed, as confirmed by DLS analysis (see below). Dactolisib was thus loaded into PEG(5400)-*b*-PAA(2000) micelles (hereafter referred to as S-dacto/m; micelles with short PAA block loaded with dactolisib) and into PEG(10 000)-*b*-PAA(3700) micelles (hereafter referred to as L-dacto/m; micelles with long PAA block loaded with dactolisib). Micellar dispersions were purified using a Millipore stirred ultrafiltration cell equipped with an Amicon mini-reservoir RC800 and a concentration/dialysis selector valve model CDS10 (molecular weight cut-off size: 100 kDa which is above the molecular weights of the free polymers) to remove noncoupled Lx-dactolisib and PEG-*b*-PAA (Figure S3, Supporting Information). Finally, the volume of the micellar dispersion was adjusted to 10.0 mL and the dispersion was stored at 4 °C until further use.

**Preparation of Fluorescently Labeled Micelles:** Micelles that were coloaded with both Lx-dactolisib and Lx-lissamine were prepared using 20 mL solution of Lx-lissamine and Lx-dactolisib at a 1:4 mol/mol ratio (Lx-lissamine =  $0.5 \times 10^{-3}$  M, Lx-dactolisib =  $2.0 \times 10^{-3}$  M) that were dissolved in water by heating at 70 °C for 20 min. After cooling to 37 °C, the Lx-lissamine/Lx-dactolisib solution was added dropwise to 20 mL of PEG(5400)-*b*-PAA(2000) or PEG(10 000)-*b*-PAA(3700) polymer solution in water of which the pH had been adjusted to 7.4 with 0.5 N NaOH and reacted as described above. The final ratio of [(Lx-lissamine) + (Lx-dactolisib)]/[AA] was (0.2 + 0.8)/2 (mol/mol). The obtained micelles are referred to as S-lissa&dacto/m (short-polymer (PEG(5400)-*b*-PAA(2000) micelles loaded with Lx-lissamine and Lx-dactolisib) and L-lissa&dacto/m (long-polymer micelles (PEG(10 000)-*b*-PAA(3700) micelles loaded with Lx-lissamine and Lx-dactolisib).

**Characterization of Micelles:** The size and size distribution of micelles at 1 mg mL<sup>-1</sup> were determined at 25 °C in water using DLS (Zetasizer Nano S, Malvern Instruments, UK) was measured using a Malvern Zetasizer Nano-Z (Malvern Instruments, UK) at 25 °C. Morphology of S-dacto/m and L-dacto/m was visualized by TEM (JEM-1400, JEOL, Japan) operated with 100 kv acceleration voltages and 40  $\mu$ A beam current. Micelles with a concentration of 1 mg mL<sup>-1</sup> in H<sub>2</sub>O were stained with uranyl acetate solution (2%, w/v) and the samples were placed on 400-mesh copper grids.

Dactolisib loading content of the micelles was determined after destruction of the micelles by incubation with KSCN, which is a strong ligand for platinum(II) coordination.<sup>[20]</sup> S-dacto/m and L-dacto/m were separately dispersed at a concentration of 2.5 mg mL<sup>-1</sup> in PBS

containing 0.5 M KSCN and 1% v/v Tween 80 (added to solubilize the released drug); samples were incubated at 80 °C for 24 h. Samples were diluted with DMF to fall in the calibration range of dactolisib (0.125–40 µg mL<sup>-1</sup>) and analyzed with UPLC as described above. Drug loading capacity (LC) was calculated using Equation (1) and loading efficiency (LE) were calculated using Equation (2)

$$LC = \frac{\text{weight of dactolisib measured}}{\text{weight of dactolisib loaded micelles}} \times 100\% \quad (1)$$

$$LE = \frac{\text{weight of dactolisib measured}}{\text{weight of dactolisib added}} \times 100\% \quad (2)$$

**Micellar Colloidal Stability:** The colloidal stability of the micelles in PBS pH 7.4 (8.2 g of NaCl, 3.1 g of Na<sub>2</sub>HPO<sub>4</sub>·12H<sub>2</sub>O, 0.3 g of NaH<sub>2</sub>PO<sub>4</sub>·2H<sub>2</sub>O per 0.5 liter) was studied using DLS. In brief, micellar dispersion (0.5 mg mL<sup>-1</sup> dactolisib in PBS) was incubated at 37 °C for 2 d. After 0, 3, 24, and 48 h, the size of undiluted samples was measured using DLS at 25 °C.

**In Vitro Release of Dactolisib:** The in vitro release of dactolisib from the micelles was studied using a dialysis method at 37 °C. Tween 80 was added to the buffer to solubilize the released dactolisib and thus maintain sink conditions. Four different media were used: (i) Milli Q water containing 1% v/v Tween 80; (ii) PBS containing 1% v/v Tween 80; (iii) PBS containing 10 × 10<sup>-3</sup> M GSH and 1% v/v Tween 80; and (iv) PBS containing 10 × 10<sup>-3</sup> M DTT and 1% v/v Tween 80. S-dacto/m and L-dacto/m micelles (1 mL dispersion corresponding to 7.2 mg mL<sup>-1</sup> dactolisib for S-dacto/m and 10.5 mg mL<sup>-1</sup> dactolisib for L-dacto/m) were transferred into dialysis tubes (Spectra-Por Float-A-Lyzer G2, MWCO 100 kDa) that were immersed into 19 mL of the different release media (compositions given above). Samples were incubated at 37 °C under constant shaking at a rotating table. Samples of 1 mL were withdrawn from the outer dialysis solution at 0, 3, 6, 16, 24, 48, 72, and 96 h and replenished with an equal volume of fresh release medium. Each experiment was repeated three times. The concentrations of released dactolisib and Lx-dactolisib in the different samples were analyzed using UPLC as described above.

**Cell Culture:** Human breast adenocarcinoma cells MCF-7 were obtained from the American Type Culture Collection (ATCC, Manassas, Virginia, USA). The cells were maintained in Dulbecco's modified Eagle's medium (DMEM) containing 10% (v/v) fetal bovine serum (FBS). The cells were cultured in an incubator with a 5% CO<sub>2</sub> humidified atmosphere at 37 °C. MCF-7 cells were grown in 25 cm<sup>2</sup> cell culture flasks and passaged once per two days.

**Cellular Uptake of Micelles:** MCF-7 cells were seeded into a 96-well plate (1 × 10<sup>4</sup> cells/well) and allowed to adhere for 24 h at 37 °C in the culture medium containing 10% FBS. Next, media were replaced by 200 µL culture medium spiked with S-lissa&dacto/m or L-lissa&dacto/m micelles at concentrations equivalent to 5 × 10<sup>-6</sup> M lissamine (corresponding to 3.6 × 10<sup>-6</sup> M PEG(5400)-b-PAA(2000) for S-lissa&dacto/m and 1.9 × 10<sup>-6</sup> M PEG(10 000)-b-PAA(3700) for L-lissa&dacto/m). Next, the cells were incubated at culture conditions for different time periods (15, 30, 60, 120, and 180 min). Fifteen min before confocal imaging, 5 µL Hoechst 33 342 (1:1000 dilution in culture medium) was added to the wells to stain the nuclei. Subsequently, the cells were washed with PBS for three times and culture plates were transferred into a Yokogawa confocal imaging platform (Model CV7000, Yokogawa, Tokyo, Japan). Digital images using 60 × oil objective were collected using two channels representing Hoechst-stained nuclei (λ<sub>ex</sub> 405 nm, λ<sub>em</sub> 445 nm) and lissamine-stained micelles (λ<sub>ex</sub> 488 nm, λ<sub>em</sub> 600 nm), respectively. Digital images (eight views per condition) were analyzed by Columbus software for semi-quantification of the red signal of lissamine in the cells.

The relationship between cellular uptake and concentration was also investigated. MCF-7 cells were seeded into 96-well plates at a density of 1 × 10<sup>4</sup> cells/well in DMEM medium containing 10% FBS (culture medium) and allowed to adhere for 24 h at 37 °C. Next, media were replaced by 200 µL culture medium spiked with dispersions of

S-lissa&dacto/m and L-lissa&dacto/m at concentrations equivalent to—2.5 to 40 × 10<sup>-6</sup> M lissamine, which correspond to 1.8, 3.6, 7.1, 14.3, and 28.6 × 10<sup>-6</sup> M PEG(5400)-b-PAA(2000) for S-lissa&dacto/m and 1.0, 1.9, 3.8, 7.7, and 15.4 × 10<sup>-6</sup> M PEG(10 000)-b-PAA(3700) for L-lissa&dacto/m. Subsequently, the nuclei of the cells were stained with Hoechst 33 342 for 30 min and confocal fluorescence images were acquired as described above.

**Cytotoxicity Assay:** MCF-7 cells were seeded at a density of 8 × 10<sup>3</sup> cells/well in culture medium into 96-well plates and cultured for 24 h. The medium was removed and 200 µL culture medium spiked with free dactolisib, S-dacto/m or L-dacto/m micelles were added to the wells at concentrations equivalent to dactolisib at a dose range of 3–1600 × 10<sup>-9</sup> M (corresponding to 0.4–228 × 10<sup>-9</sup> M PEG(5400)-b-PAA(2000) for S-dacto/m and 0.2–123 × 10<sup>-9</sup> M PEG(10 000)-b-PAA(3700) for L-dacto/m). The cells were incubated for another 72 h and then 40 µL of MTS (inner salt) reagent was added to the wells. Subsequently, the cells were incubated for another 4 h at 37 °C. The absorbance at 492 nm was recorded using a microplate reader (Thermoscientific Multiskan MK3). The cytotoxicity of dactolisib is expressed as the percentage of viable cells compared to untreated control cells.

**PI3K/mTOR Signaling Pathway Phospho-Western Blot Evaluation:** Specific inhibitory activity of dactolisib was determined by phospho-Western blot analysis of proteins downstream in the PI3K/mTOR signaling pathway: phospho-Akt (Ser473) and phospho-S6 ribosomal protein (Ser240/244), respectively.<sup>[6c]</sup> β-Actin was stained to confirm the equal lane loading of protein in the gels. In brief, MCF-7 cells were seeded into 6-well plates (2 × 10<sup>5</sup> cells/well; Falcon) and allowed to adhere overnight in the culture medium containing 10% FBS. Next, the cells were incubated with culture medium containing free dactolisib, S-dacto/m or L-dacto/m micelles at concentrations equivalent to dactolisib 200–400 × 10<sup>-9</sup> M (corresponding to 28–56 × 10<sup>-9</sup> M PEG(5400)-b-PAA(2000) for S-dacto/m and 15–30 × 10<sup>-9</sup> M PEG(10 000)-b-PAA(3700) for L-dacto/m). The cells were incubated for 16 h at 37 °C, followed by washing with cold PBS and subsequent lysis with radio-immunoprecipitation assay buffer (RIPA), supplemented with phosphatase/kinase inhibitor cocktail (ThermoFisher, Bleiswijk, the Netherlands) on ice for 30 min.<sup>[34]</sup> The resulting cell lysates were centrifuged at 12 000 × g for 15 min and the protein concentration in the supernatants was quantified using the Pierce bicinchoninic acid (BCA) protein assay kit. Samples were loaded at equal amounts of protein (20 µg) onto SDS-PAGE (sodium dodecyl sulfate polyacrylamide gel electrophoresis) 4%–12% Bis-Tris gels and separated by electrophoresis on a miniProtein system (Biorad). Next, the gel was transferred onto nitrocellulose membranes by iBlot dry blotting method.<sup>[26]</sup> After blocking with 5% milk in TBST [20 × 10<sup>-3</sup> M tris (pH 7.6), 150 × 10<sup>-3</sup> M NaCl and 0.1% Tween 20] at room temperature for 1 h, the membranes were incubated with primary antibodies phospho-S6 ribosomal protein (Ser240/244) rabbit mAb, phospho-Akt (Ser473) rabbit mAb, and β-Actin rabbit mAb overnight at 4 °C.<sup>[7c,35]</sup> Next, the membranes were washed three times with TBST and incubated with goat anti-rabbit horseradish peroxidase (HRP)-conjugated secondary antibody at room temperature for 1 h. After three washings with the TBST buffer, protein expression was visualized by using the enhanced chemiluminescence (ECL) Western blotting reagent and the membranes were scanned with a Gel Doc Imaging system equipped with one XRS camera.

**Statistical Analysis:** GraphPad Prism software version 7 (GraphPad Software, Inc.) was used for statistical analysis. All experimental data are presented as mean ± standard deviation. Two-way analysis of variance (ANOVA) was used to determine significance between groups. Statistical significance differences are considered when *P* value < 0.05.

## Supporting Information

Supporting Information is available from the Wiley Online Library or from the author.

## Acknowledgements

This work was supported by the China Scholarship Council (CSC).

## Conflict of Interest

The authors declare no conflict of interest.

## Keywords

coordination chemistry, drug delivery, kinase inhibitors, polymeric micelles, polymer–metal complexes

Received: June 5, 2019  
Published online: July 28, 2019

- [1] a) T. Lammers, F. Kiessling, W. E. Hennink, G. Storm, *J. Controlled Release* **2012**, 161, 175; b) E. Blanco, H. Shen, M. Ferrari, *Nat. Biotechnol.* **2015**, 33, 941.
- [2] a) V. P. Torchilin, *Nat. Rev. Drug Discovery* **2014**, 13, 813; b) C. J. Cheng, G. T. Tietjen, J. K. Saucier-Sawyer, W. M. Saltzman, *Nat. Rev. Drug Discovery* **2015**, 14, 239; c) J. A. Hubbell, A. Chilkoti, *Science* **2012**, 337, 303; d) L. Houdaihed, J. C. Evans, C. Allen, *Mol. Pharmaceutics* **2017**, 14, 2503.
- [3] a) H. Cabral, K. Kataoka, *J. Controlled Release* **2014**, 190, 465; b) C. Deng, Y. Jiang, R. Cheng, F. Meng, Z. Zhong, *Nano Today* **2012**, 7, 467; c) Y. Shi, T. Lammers, G. Storm, W. E. Hennink, *Macromol. Biosci.* **2017**, 17, 1600160; d) S. Eetezadi, S. N. Ekdawi, C. Allen, *Adv. Drug Delivery Rev.* **2015**, 91, 7.
- [4] a) J. Fang, H. Nakamura, H. Maeda, *Adv. Drug Delivery Rev.* **2011**, 63, 136; b) H. Maeda, J. Wu, T. Sawa, Y. Matsumura, K. Hori, *J. Controlled Release* **2000**, 65, 271.
- [5] a) M. Murakami, H. Cabral, Y. Matsumoto, S. Wu, M. R. Kano, T. Yamori, N. Nishiyama, K. Kataoka, *Sci. Transl. Med.* **2011**, 3, 64ra2; b) Q. Yin, J. Shen, Z. Zhang, H. Yu, Y. Li, *Adv. Drug Delivery Rev.* **2013**, 65, 1699; c) A. Ganoth, K. C. Merimi, P. Dan, *Expert Opin. Drug Delivery* **2015**, 12, 223.
- [6] a) V. Serra, B. Markman, M. Scaltriti, P. J. Eichhorn, V. Valero, M. Guzman, M. L. Botero, E. Llonch, F. Atzori, S. Di Cosimo, M. Maira, C. Garcia-Echeverria, J. L. Parra, J. Arribas, J. Baselga, *Cancer Res.* **2008**, 68, 8022; b) B. Gobin, S. Battaglia, R. Lanel, J. Chesneau, J. Amiaud, F. R dini, B. Ory, D. Heymann, *Cancer Lett.* **2014**, 344, 291; c) T.-J. Liu, D. Koul, T. LaFortune, N. Tiao, R. J. Shen, S.-M. Maira, C. Garcia-Echeverria, W. K. A. Yung, *Mol. Cancer Ther.* **2009**, 8, 2204.
- [7] a) R. Marone, D. Erhart, A. C. Mertz, T. Bohnacker, C. Schnell, V. Cmiljanovic, F. Stauffer, C. Garcia-Echeverria, B. Giese, S. M. Maira, M. P. Wymann, *Mol. Cancer Res.* **2009**, 7, 601; b) S. M. Maira, F. Stauffer, J. Brueggen, P. Furet, C. Schnell, C. Fritsch, S. Brachmann, P. Chene, A. De Pover, K. Schoemaker, D. Fabbro, D. Gabriel, M. Simonen, L. Murphy, P. Finan, W. Sellers, C. Garcia-Echeverria, *Mol. Cancer Ther.* **2008**, 7, 1851; c) A. C. Faber, D. Li, Y. Song, M.-C. Liang, B. Y. Yeap, R. T. Bronson, E. Lifshits, Z. Chen, S.-M. Maira, C. Garcia-Echeverria, K. K. Wong, J. A. Engelman, *Proc. Natl. Acad. Sci. USA* **2009**, 106, 19503.
- [8] a) R. Salazar, R. Garcia-Carbonero, S. K. Libutti, A. E. Hendifar, A. Custodio, R. Guimbaud, C. Lombard-Bohas, S. Ricci, H. J. Klumpen, J. Capdevila, N. Reed, A. Walenkamp, E. Grande, S. Safina, T. Meyer, O. Kong, H. Salomon, R. Tavorath, J. C. Yao, *Oncologist* **2018**, 23, 766; b) M. I. Carlo, A. M. Molina, Y. Lakhman, S. Patil, K. Woo, J. DeLuca, C.-H. Lee, J. J. Hsieh, D. R. Feldman, R. J. Motzer, M. H. Voss, *Oncologist* **2016**, 21, 787.
- [9] a) A. Kolate, D. Baradia, S. Patil, I. Vhora, G. Kore, A. Misra, *J. Controlled Release* **2014**, 192, 67; b) S. A. Senevirathne, K. E. Washington, J. B. Miller, M. C. Biewer, D. Oupicky, D. J. Siegwart, M. C. Stefan, *J. Mater. Chem. B* **2017**, 5, 2106; c) O. Soga, C. F. van Nostrum, A. Ramzi, T. Visser, F. Soulimani, P. M. Frederik, P. H. Bomans, W. E. Hennink, *Langmuir* **2004**, 20, 9388.
- [10] a) E. S. Yim, Z. Betty, M. David, L. C. Kourtis, C. W. Frank, C. Dennis, R. L. Smith, S. B. Goodman, *J. Biomed. Mater. Res., Part A* **2009**, 91A, 894; b) N. Ahmad, M. C. Amin, S. M. Mahali, I. Ismail, V. T. Chuang, *Mol. Pharmaceutics* **2014**, 11, 4130; c) M. Xu, J. Zhu, F. Wang, Y. Xiong, Y. Wu, Q. Wang, J. Weng, Z. Zhang, W. Chen, S. Liu, *ACS Nano* **2016**, 10, 3267.
- [11] a) B. Lev, *Expert Opin. Drug Delivery* **2005**, 2, 1003; b) R. Barreiro-Iglesias, L. Bromberg, M. Temchenko, T. A. Hatton, C. Alvarez-Lorenzo, A. Concheiro, *Eur. J. Pharm. Sci.* **2005**, 26, 374; c) M. Wahlgren, K. L. Christensen, E. V. Jorgensen, A. Svensson, S. Ulvenlund, *Drug Dev. Ind. Pharm.* **2009**, 35, 922; d) A.-M. Vasi, M. I. Popa, E. C. Tanase, M. Butnaru, L. Verestiuc, *J. Pharm. Sci.* **2014**, 103, 676.
- [12] a) H. Uchino, Y. Matsumura, T. Negishi, F. Koizumi, T. Hayashi, T. Honda, N. Nishiyama, K. Kataoka, S. Naito, T. Kakizoe, *Br. J. Cancer* **2005**, 93, 678; b) H. Cabral, N. Nishiyama, K. Kataoka, *J. Controlled Release* **2007**, 121, 146.
- [13] H. Shi, W. N. Leonhard, N. J. Sijbrandi, M. J. van Steenberg, M. H. Fens, J. B. van de Dikkenberg, J. S. Tor no, D. J. Peters, W. E. Hennink, R. J. Kok, *J. Controlled Rel.* **2019**, 293, 113.
- [14] a) N. J. Sijbrandi, E. Merkul, J. A. Muns, D. C. Waalboer, K. Adamzek, M. Bolijn, V. Montserrat, G. W. Somsen, R. Haselberg, P. J. Steverink, H. J. Houthoff, G. A. van Dongen, *Cancer Res.* **2017**, 77, 257; b) D. C. Waalboer, J. A. Muns, N. J. Sijbrandi, R. B. Schasfoort, R. Haselberg, G. W. Somsen, H. J. Houthoff, G. A. van Dongen, *ChemMedChem* **2015**, 10, 797; c) S. Harmsen, M. E. Dolman, Z. Nemes, M. Lacombe, B. Szokol, J. Pato, G. Keri, L. Orfi, G. Storm, W. E. Hennink, R. J. Kok, *Bioconjugate Chem.* **2011**, 22, 540; d) K. Temming, M. Lacombe, P. van der Hoeven, J. Prakash, T. Gonzalo, E. C. Dijkers, L. Orfi, G. K ri, K. Poelstra, G. Molema, R. J. Kok, *Bioconjugate Chem.* **2006**, 17, 1246; e) M. Dolman, K. Van Dorenmalen, E. Pieters, M. Lacombe, J. Pato, G. Storm, W. Hennink, R. J. Kok, *J. Controlled Release* **2012**, 157, 461.
- [15] a) C. Barner-Kowollik, M. Buback, B. Charleux, M. L. Coote, M. Drache, T. Fukuda, A. Goto, B. Klumperman, A. B. Lowe, J. B. Mcleary, *J. Polym. Sci., Part A: Polym. Chem.* **2006**, 44, 5809; b) W. A. Braunecker, K. Matyjaszewski, *Prog. Polym. Sci.* **2007**, 32, 93.
- [16] M. Chen, G. Moad, E. Rizzardo, *J. Polym. Sci., Part A: Polym. Chem.* **2009**, 47, 6704.
- [17] Y. Mochida, H. Cabral, Y. Miura, F. Albertini, S. Fukushima, K. Osada, N. Nishiyama, K. Kataoka, *ACS Nano* **2014**, 8, 6724.
- [18] a) S. Bhattacharjee, *J. Controlled Release* **2016**, 235, 337; b) S. Bhattacharjee, *J. Controlled Release* **2016**, 238, 311.
- [19] J. Makino, H. Cabral, Y. Miura, Y. Matsumoto, M. Wang, H. Kinoh, Y. Mochida, N. Nishiyama, K. Kataoka, *J. Controlled Release* **2015**, 220, 783.
- [20] M. M. Fretz, M. E. Dolman, M. Lacombe, J. Prakash, T. Q. Nguyen, R. Goldschmeding, J. Pato, G. Storm, W. E. Hennink, R. J. Kok, *J. Controlled Release* **2008**, 132, 200.
- [21] H. Cabral, Y. Matsumoto, K. Mizuno, Q. Chen, M. Murakami, M. Kimura, Y. Terada, M. R. Kano, K. Miyazono, M. Uesaka, N. Nishiyama, K. Kataoka, *Nat. Nanotechnol.* **2011**, 6, 815.
- [22] a) T. Gonzalo, E. G. Talman, A. van de Ven, K. Temming, R. Greupink, L. Beljaars, C. Reker-Smit, D. K. Meijer, G. Molema, K. Poelstra, R. J. Kok, *J. Controlled Release* **2006**, 111, 193; b) M. E. Dolman, K. M. van Dorenmalen, E. H. Pieters, R. W. Sparidans, M. Lacombe,

- B. Szokol, L. Orfi, G. Keri, N. Bovenschen, G. Storm, W. E. Hennink, R. J. Kok, *Macromol. Biosci.* **2012**, *12*, 93.
- [23] a) N. Nishiyama, S. Okazaki, H. Cabral, M. Miyamoto, Y. Kato, Y. Sugiyama, K. Nishio, Y. Matsumura, K. Kataoka, *Cancer Res.* **2003**, *63*, 8977; b) H. Cabral, N. Nishiyama, S. Okazaki, H. Koyama, K. Kataoka, *J. Controlled Release* **2005**, *101*, 223.
- [24] Y. Bae, S. Fukushima, A. Harada, K. Kataoka, *Angew. Chem., Int. Ed.* **2003**, *42*, 4640.
- [25] a) L. Jiang, X. Li, L. Liu, Q. Zhang, *Int. J. Nanomed.* **2013**, *8*, 1825; b) Q. Sun, T. Ishii, K. Kanehira, T. Sato, A. Taniguchi, *Biomater. Sci.* **2017**, *5*, 1014.
- [26] Z. Yu, G. Xie, G. Zhou, Y. Cheng, G. Zhang, G. Yao, Y. Chen, Y. Li, G. Zhao, *Cancer Lett.* **2015**, *367*, 58.
- [27] R. Savić, T. Azzam, A. Adi Eisenberg, D. Maysinger, *Langmuir* **2006**, *22*, 3570.
- [28] a) Y. Shi, R. Van Der Meel, B. Theek, E. Oude Blenke, E. H. Pieters, M. H. Fens, J. Ehling, R. M. Schiffelers, G. Storm, C. F. van Nostrum, T. Lammers, W. E. Hennink, *ACS Nano* **2015**, *9*, 3740; b) Y. Shi, M. J. V. Steenbergen, E. A. Teunissen, L. S. Novo, S. Gradmann, M. Baldus, C. F. van Nostrum, W. E. Hennink, *Biomacromolecules* **2013**, *14*, 1826.
- [29] a) N. Nishiyama, Y. Kato, Y. Sugiyama, K. Kataoka, *Pharm. Res.* **2001**, *18*, 1035; b) H. Cabral, K. Miyata, K. Osada, K. Kataoka, *Chem. Rev.* **2018**, *118*, 6844.
- [30] S. Buwalda, B. Nottelet, A. Bethry, R. J. Kok, N. Sijbrandi, J. Coudane, *J. Colloid Interface Sci.* **2019**, *535*, 505.
- [31] a) I. Chaduc, A. Crepet, O. Boyron, B. Charleux, F. D'Agosto, M. Lansalot, *Macromolecules* **2013**, *46*, 6013; b) L. Ouyang, L. Wang, F. J. Schork, *Macromol. React. Eng.* **2011**, *5*, 163.
- [32] G. Moad, Rizzardo, E., Thang, S. H., *Polym. Int.* **2011**, *60*, 9.
- [33] M. Yokoyama, T. Okano, Y. Sakurai, S. Suwa, K. Kataoka, *J. Controlled Release* **1996**, *39*, 351.
- [34] S. Gholizadeh, J. A. Kamps, W. E. Hennink, R. J. Kok, *Int. J. Pharm.* **2018**, *548*, 747.
- [35] Z. Sun, Q. Li, S. Zhang, J. Chen, L. Huang, J. Ren, Y. Chang, Y. Liang, G. Wu, *OncoTargets Ther.* **2015**, *8*, 269.